Annual Progress Report

NASA Grant NGR-33-010-057

for

IMPROVEMENTS TO EMBEDDED SHOCK WAVE CALCULATIONS FOR TRANSONIC FLOW-APPLICATIONS TO WAVE DRAG AND PRESSURE RISE PREDICTIONS

from

Cornell University
Ithaca, N. Y. 14850

Principal Investigator: A. R. Seebass

Research Associate: N. J. Yu

Technical Officer: Leroy L. Presley
NASA Ames Research Center

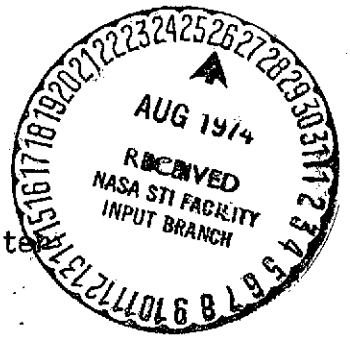

Contents:

August 1974

1. Review

a. Physical problems and test computations

Our research has concentrated on the numerical "solution" of a single, mixed, nonlinear equation with prescribed boundary data. The governing equation has the general form

$$\{C(y) + \phi_x\}\,\phi_{xx} - \phi_{yy} = 0 \tag{1}$$

For the caustic problem, which we examined first, $C(y)$ has the simple form

$$C(y) = y, \tag{2}$$

and the boundary data are prescribed in accordance with the asymptotic analog of (1), viz.,

$$y\phi_{xx} - \phi_{yy} = 0. \tag{3a}$$

These boundary data include an incoming signal,

$$\phi_x = -\mu_y^{-1/4} F(p), \text{ along } q = -1, \tag{3b}$$

where $F(p)$ gives the shape of the incoming signal, μ characterizes its strength, and $p,q = x \pm \frac{2}{3} y^{3/2}$, respectively.

For the two-dimensional transonic flow problems, which we are now investigating, $C(y)$ is the constant transonic parameter, $-K$. The boundary data here are the far-field behavior of the solution and the tangency condition on the airfoil.

We have developed a second-order numerical procedure for "solving" (1) and a shock-fitting scheme to treat the discontinuities that appear in the solution. Numerical results for this (the caustic) problem are codified in the appended paper, which will be delivered at the First International Conference on Computational Method in Nonlinear Mechanics, September 23-25, 1974.

In the following sections, we outline the research progress we have made to date and further work now underway. These include a brief review of the second order scheme, the shock fitting technique, comparison of the results of various schemes, and a preliminary test computation of a transonic flow problem.

b. Second-order scheme

The second-order scheme which is used in the present computation is similar to the first-order scheme of Murman and Cole (1971), i.e., in elliptic regions ($C(y) + \phi_x < 0$) a central difference approximation is chosen to represent the x- and the y-derivatives:

$$\begin{aligned} \phi_x &= (\phi_{i+1,j} - \phi_{i-1,j})/2\,\Delta x \ , \\ \phi_{xx} &= (\phi_{i+1,j} - 2\phi_{i,j} + \phi_{i-1,j})/\Delta x^2 \ , \\ \phi_{yy} &= (\phi_{i,j+1} - 2\phi_{i,j} + \phi_{i,j-1})/\Delta y^2 \ . \end{aligned} \tag{4a}$$

In hyperbolic regions ($C(y) + \phi_x > 0$) the x-derivatives are replaced by one-sided differences to correctly represent the domain of dependence,

$$\begin{aligned} \phi_x &= (2\phi_{i,j} - \phi_{i-1,j} - 2\phi_{i-2,j} + \phi_{i-3,j})/2\Delta x \ , \\ \phi_{xx} &= (2\phi_{i,j} - 5\phi_{i-1,j} + 4\phi_{i-2,j} - \phi_{i-3,j})/\Delta x^2 \ . \end{aligned} \tag{4b}$$

After substituting (4a) and (4b) into (1), we obtain a set of nonlinear difference equations of the form

$$A_1\,\phi^{n+1}_{i,j+1} + A_2\,\phi^{n+1}_{i,j} + A_3\,\phi^{n+1}_{i,j-1} + A_5 = F_j(\phi) = 0 \ . \tag{5}$$

The coefficients An, are shown in Table 1 of the appended paper. Equation (5) is flux conservative; we solve it by the Newton's method:

$$(\phi^{n+1} - \phi^n)\ \partial F_j/\partial \phi_k = -\,F_j(\phi) \ . \tag{6}$$

In our last report we pointed out that the matrix $\partial F_j/\partial \phi_k$ loses diagonal dominance in hyperbolic compressive regions, which causes poor convergence or instability in the iterative procedure when the initial guess is not accurate. We remedied this by introducing an artificial viscosity, $\nu\phi_{xxx}$, such that (1) becomes

$$\{C(y) + \phi_x\}\phi_{xx} - \phi_{yy} = \nu\phi_{xxx} \ . \tag{7}$$

The diagonal term of (6) becomes

$$\partial F_j/\partial \phi_j = \frac{2}{\Delta y^2} + \frac{2}{\Delta x^2}\{C(y) + \phi_x\} + \frac{1}{\Delta x}\phi_{xx} + \nu/\Delta x^3 \ ; \tag{8}$$

ν is zero when

$$\frac{2}{\Delta x^2}\{C(y) + \phi_x\} + \frac{1}{\Delta x}\phi_{xx} > 0 \ . \tag{9a}$$

When this is not the case, we choose

$$\nu = k\Delta x^2\left\{\frac{2}{\Delta x}[C(y) + \phi_x] + \phi_{xx}\right\} , \tag{9b}$$

where $k > 1$.

With this modification, equation (6) has diagonal dominance everywhere in the computational field. Test computations show that the present scheme provides a converged solution for a wide range of signal strengths (μ = 0.05 to 0.25) with the linear solution to (3a) as an initial guess. After the numerical value of $\phi_{i,j}$ becomes more accurate (usually about 20 computations*), we can set $\nu = 0$ and continue the computational procedure without difficulty until the "solution" converges. The results for our second-order calculation for signal strength of $\mu = 0.05$ are displayed in Figure 3 of the appendix.

*A computation is one complete calculation of the flow field.

c. Shock fitting scheme for the caustic problem

Usual finite difference schemes give poor representations of flow fields with shock waves embedded in them. This is the consequence of replacing derivatives by difference approximations in the whole computation region regardless of the discontinuous behavior of the solution. A correct "solution" can only be obtained by treating shocks as a discontinuity. Moretti (1972,1973) has emphasized the importance of shock fitting for flows containing shock waves in several of his papers. Without shock fitting a large number of grid points and considerable computing time are required to achieve a given accuracy. In the appendix we demonstrate the computational advantage of shock-fitting scheme by studying the nonlinear acoustic behavior of a shock wave near a caustic using different numerical schemes. The difficulties associated with shock fitting include determining the location of the shock and simplifying the numerical program so that it can be easily used. We have developed a successful scheme to solve the caustic problem; for other applications, our results require proper generalization.

We assume a discontinuous signal with prescribed shape and strength given by (3b). The initial position of the signal (shock) is known (Figure 1 of the appendix) and the successive position of the shock along each computation column $x = x_i$ is determined by

$$(dy/dx)_s = \pm \{C(y) + \frac{1}{2}(\phi_x + \hat{\phi}_x)\}^{-1/2} . \qquad (10)$$

The flow properties ahead of the shock are obtained by the characteristic relations

$$\{C(y) + \phi_x\}^{1/2} d\phi_x = \pm d\phi_y , \qquad (11)$$

and the flow properties right behind the shock are determined by one of equations (11) and the jump condition

$$(\hat{\phi}_x - \phi_x)^2 \{C(y) + \frac{1}{2}(\phi_x + \hat{\phi}_x)\} = (\hat{\phi}_y - \phi_y)^2 . \qquad (12)$$

Table 2 of the appendix details the procedure used to compute the position of shock and determine ϕ, ϕ_x, ϕ_y at the shock.

Difference equations are then constructed by considering the shock point as a grid point. The entire difference equations including both shock, and shock free, regions are listed in Table 1 of the appendix. At every computation point, the type dependent coefficient, $C(y) + \phi_x$ is evaluated by a central difference approximation. At the same time, the position of the shock is detected such that the proper difference equation can be chosen. The difference equation in shock region is not in conservative form, since such a form is not possible. Internal sources or sinks due to the nonconservative approximation are localized and can be considered negligible as we have avoided differencing across sharp gradients.

In the region where the downstream condition of the shock becomes subsonic, equation (11) is no longer valid and we have to evaluate the flow property, e.g., $\hat{\phi}_x$, by a one-sided difference approximation, and calculate $\hat{\phi}_y$ by (12).

As the incident shock reaches the sonic line, i.e., $C(y) + \phi_x = 0$, we assume a reflected wave is formed. The initial strength of the reflected shock is obtained by using backward differences to approximate properties ahead of the shock and using forward differences to approximate properties behind the shock. With such an approximation, the reflected shock is quite weak. We have tried local symmetrical shocks at the triple point as proposed in the last progress report, but these do not seem to have the correct properties as we have not obtained a converged solution using them. A more general triple-point model is now under investigation.

Computer drawn plots of ϕ_x/μ at different y are shown in Figure 5 of the appendix.

2. Comparisons of various schemes

In Figure 2 of the appendix the linear solution of equation (3) for $\mu = 0.05$, and $\delta = 20$ (Gill and Seebass, 1974) is reproduced. This serves as an initial guess for our second-order scheme. Figure 4 of the appendix shows the first-order numerical results of Seebass, Murman, and Krupp (1971). First-order truncation errors diffuse the shock waves, especially near triple point where the incident shock and the reflected shock can not be clearly distinguished. Figure 3 of the appendix is the result obtained by the present second-order scheme. The shock waves become sharper and the amplitude of the shock jump increases. However, in the region where dispersive errors dominate, i.e., $|C(y) + \phi_x| > |\phi_{xx}|$, an unpleasant "wiggle" appears downstream of the shock. Such phenomenon can be eliminated by fitting a shock wave that satisfies the correct jump relations. Figure 5 of the appendix shows the result of the shock-fitting scheme after 20 computations from the converged second-order "solution". The dispersive "wiggle" vanishes after the first computation with the shock-fitting scheme. Table 3 of the appendix shows the differences in computing time and the rate of convergence for different schemes. Compared with the first-order and the second-order schemes, computing time per computation with the shock-fitting scheme is doubled, but the total computing time to bring the result to the same final accuracy is appreciably reduced. The fast rate of convergence and the correct shock jump are the main advantages of our shock fitting scheme.

3. Transonic flow over two dimensional airfoils

a. Governing equation

The first-order approximation for transonic flow over a thin airfoil is

$$(K - \phi_x)\,\phi_{xx} + \phi_{\eta\eta} = 0, \tag{13}$$

where K is the transonic similarity parameter, and is defined as

$$K = (1 - M_\infty^2)/(2\Gamma_1\,\tau\,M_\infty^2)^{2/3}, \tag{14}$$

and ϕ is the nondimensional perturbed velocity potential, which is related to the perturbed velocities u', v', by

$$\phi_x = \frac{(2\Gamma_1\,M_\infty^2)^{1/3}}{\tau^{2/3}}\,(u'/U_\infty) \tag{15a}$$

$$\phi_\eta = \frac{1}{\tau}\,(v'/U_\infty). \tag{15b}$$

Here τ is the thickness ratio, $\Gamma_1 = (\gamma + 1)/2$, x, η are related to the physical coordinates by

$$x = x/c, \qquad \eta = (2\Gamma_1\,\tau\,M_\infty^2)^{1/3}\,y/c, \tag{16}$$

where c is the chord length.

The boundary conditions are then on $y = \tau\,Y(x)$, or $\eta \to 0$

$$\phi_\eta = Y'(x), \tag{17a}$$

and at infinity,

$$\phi_x\ ,\ \phi_\eta \to 0$$

for $$M_\infty < 1\ . \tag{17b}$$

For $M_\infty > 1$ far-field boundary data are calculated by the method of characteristics. For example, at boundary point B in the following sketch, we have

$$(\phi_x - K_s)^{3/2}\,d\,\phi_x = -\,d\,\phi_\eta,$$

or

$$2/3\,\{(\phi_x - K_s)_B^{3/2} - (\phi_x - K_{s_\infty})^{3/2}\} = -\,\phi_{\eta B} + \phi_{\eta\infty}$$

along the characteristic C_2.

Both $\phi_{x\infty}$ and $\phi_{\eta\infty}$ are zero on C_2, thus

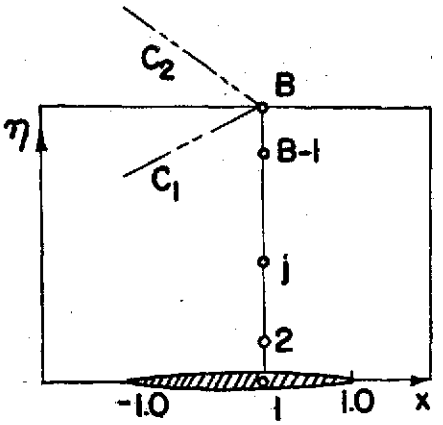

$$\phi_{\eta B} = \frac{2}{3}\{(-K)^{3/2} - (\phi_x - K)_B^{3/2}\}. \quad (17c)$$

Using (13), we can calculate ϕ_B by a one-sided difference approximation, i.e.,

$$\phi_{\eta\eta_B} = \frac{2}{\Delta\eta}\left\{\phi_{\eta_B} - \phi_{\eta_{B-1/2}}\right\} = \frac{2}{\Delta\eta}\left\{\phi_{\eta_B} - \frac{1}{\Delta\eta}(\phi_B - \phi_{B-1})\right\}$$

$$= \frac{2}{\Delta\eta}\left\{\frac{2}{3}\left[(-K)^{3/2} - (\phi_{x_B} - K)^{3/2}\right] - \frac{1}{\Delta\eta}(\phi_B - \phi_{B-1})\right\}, \quad (17d)$$

where ϕ_{x_B} is computed by a backward difference approximation.

For a finite computation region, the far field boundary data for $M_\infty < 1$ are obtained by using the formula derived by Murman and Cole (1971),

$$\phi = \frac{1}{2\pi\sqrt{K}}\left\{2\int_{-1}^{1}\frac{x-\xi}{(x-\xi)^2+K\eta^2}Y(\xi)d\xi + \frac{1}{2}\frac{x}{x^2+K\eta^2}\iint_{-\infty}^{\infty}\phi_x^2\,d\xi d\eta\right\}. \quad (18)$$

The first term in (18) is the traditional Prandtl-Glauert solution for the linear asymptotic analog of (13); and the second term is the nonlinear correction due to the perturbed velocity ϕ_x.

On the airfoil $\phi_{\eta\eta}$ is approximated by a reflected boundary condition, i.e.,

$$\phi_{\eta\eta_1} = \frac{1}{\Delta\eta^2}(\phi_2 - 2\phi_1 + \phi_o) = \frac{1}{\Delta\eta^2}\left\{2(\phi_2 - \phi_1) - 2\Delta\eta\,\phi_{\eta_1}\right\}, \quad (19)$$

where subscript "1" refers to the point on the body.

The same numerical procedure discussed in section 1 is followed. A test computation for a 6% thick parabolic, nonlifting airfoil at various Mach numbers has been carried out. For subsonic flow over the airfoil, the far field solution is corrected after every 5 forward computations. At the same

time the computation procedure is reversed, i.e., from downstream to upstream, to bring the effect of the downstream boundary condition to the whole flow field as soon as practicable. Converged solutions have been obtained using our second-order scheme for M_∞ = 0.806, 0.861, 0.909. Figure 1 shows the present results, the results of first-order computation, and the results of Murman (1974). There is a major discrepancy in the shock wave position between our results and those calculated by Murman. This results in a large disagreement in the wave drag:

Murman and Cole (1974):	C_D = 0.0315
Present:	0.0125
Knetchtel:	0.00835

This discrepancy could be attributed to our use of a normal shock on the shock-fitting scheme, but initial calculations which allow for a floating shock of general shape, locate the shock at $x/c = 0.875 \pm 0.025$. This disagreement needs to be resolved and we are in the process of refining our calculations in order to do so.

b. Embedded shock

For supercritical flow, i.e., subsonic flow with embedded supersonic region, a shock wave is formed near the trailing edge through coalescence of waves originating on the body and reflected from the sonic line. Numerical results for the 6% parabolic arc airfoil show a rapid compression region near the trailing edge for $M_\infty > 0.85$. Correct representation of embedded shock requires a shock-fitting scheme. We assume the shock originates in far-field with infinitesimal strength, where the position of the shock is determined by the following criteria:

$$(K - \phi_x)_c = 0^+, \text{ and } (K - \phi_x)_b = 0^- ; \qquad (20)$$

the subscript "c" refers to the quantity evaluated by central difference

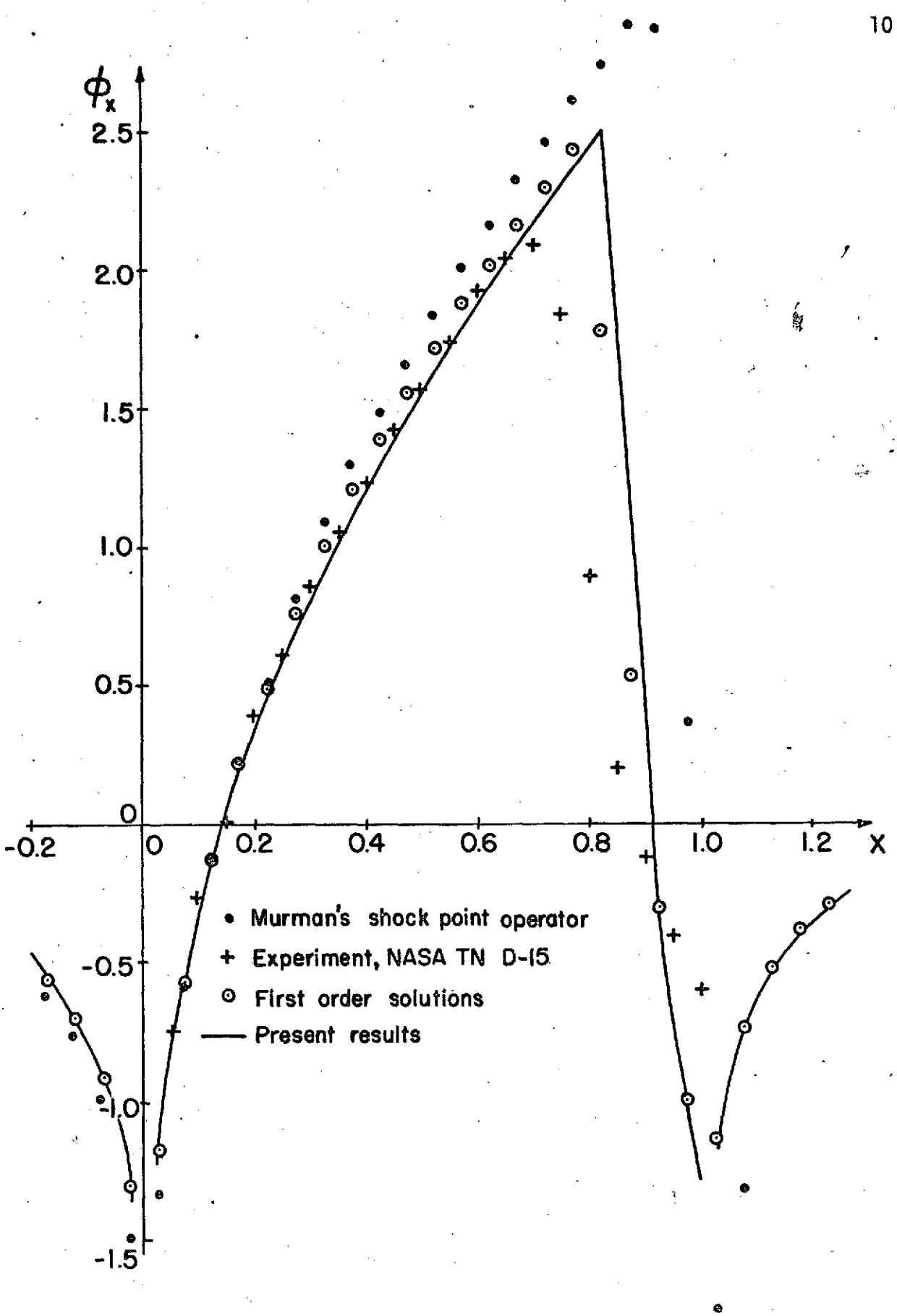

Fig. 1. ϕ_x vs. x for 6% arc nonlifting airfoil at $M_\infty = 0.909$, $\eta = 0$.

approximation, and "b" the backward difference approximation. This criteria is equivalent to insisting that the shock form in a supersonic, compression region. Once the starting point of the shock is determined, we can then trace out the shock position by the procedure of section 1c. Our preliminary computations have been limited to fitting a normal shock throughout the flow field. This is not a true representation of the shock that appears in the flow, but it provides some qualitative features of the flow field. Figure 2 shows the velocity variation at different η for $M_\infty = 0.909$. An expansion occurs behind the shock; this probably corresponds to the Zierep (1958) singularity which does not show up in many numerical results. A floating shock fitting scheme is now under investigation.

c. Wave drag

Transonic wave drag can either be calculated by a contour integration of the pressure around the airfoil, or by the entropy production due to shock waves. Murman and Cole (1974) have pointed out that due to the leading edge singularity, the embedded shock waves, and the fast variation of pressure near trailing edge, an accurate drag is hard to obtain by contour integration around the body. The alternative method is to compute the entropy production due to shock waves, and then to apply Oswatitsch's drag formula to determine the wave drag,

$$D = \lim_{X\to\infty} \rho_\infty T_\infty \int_{-\infty}^{\infty} (s - s_\infty)\, dy$$

$$= \rho_\infty T_\infty \int_{\text{shocks}} (\Delta s)_{\text{shock}}\, dy. \qquad (21)$$

We know that (13) is the correct first-order approximation for transonic flow over a thin airfoil in the domain where shock waves and other discontinuities

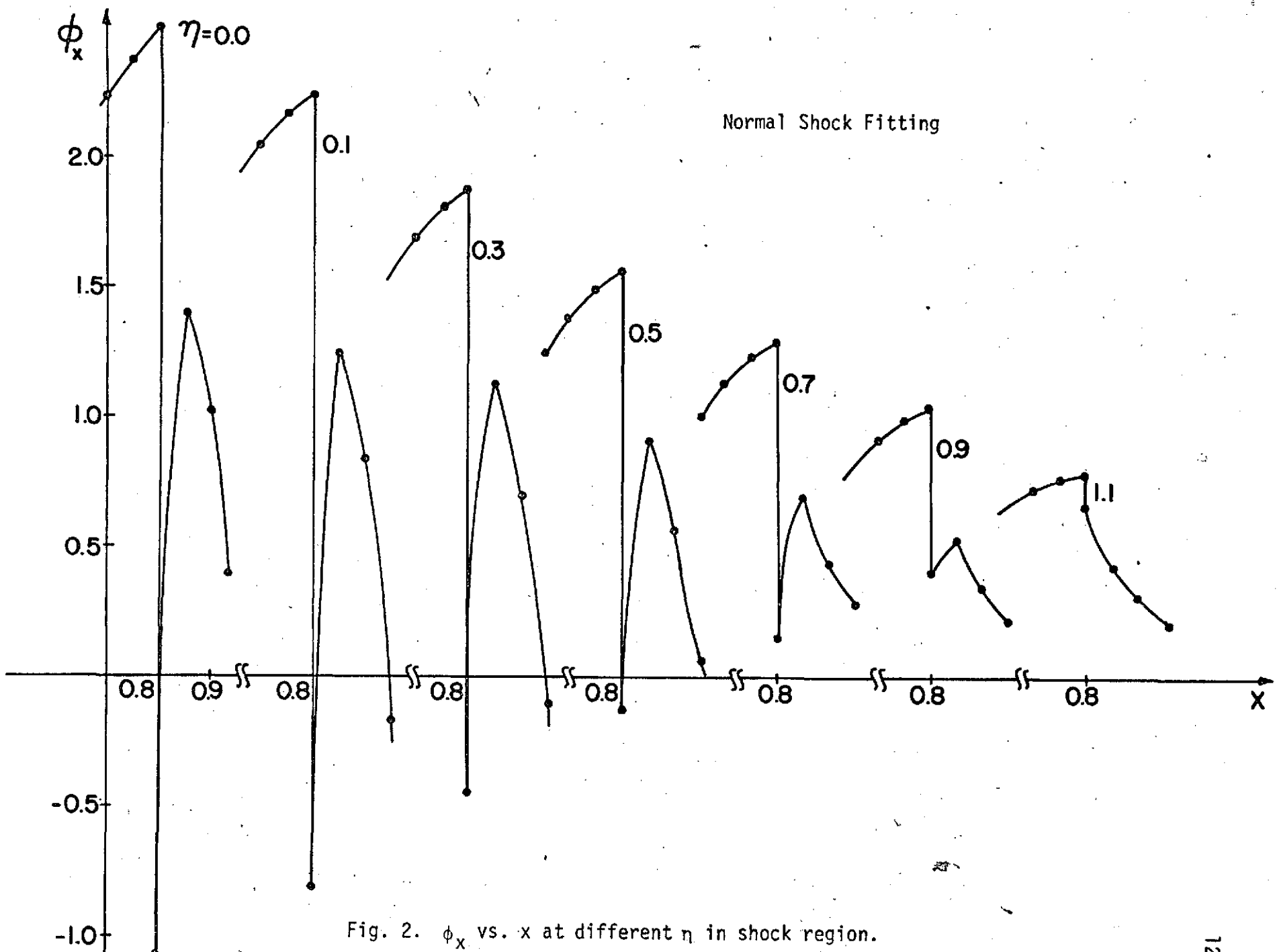

Fig. 2. ϕ_x vs. x at different η in shock region.
6% arc, M_∞ = 0.909.

are excluded. In the sketch, S represents the shock, W the wake, and B the airfoil. D is the domain where (13) applies. A weak solution of (13) provides a proper jump in pressure and velocity across S, which can be used to relate to the entropy change to the pressure jump:

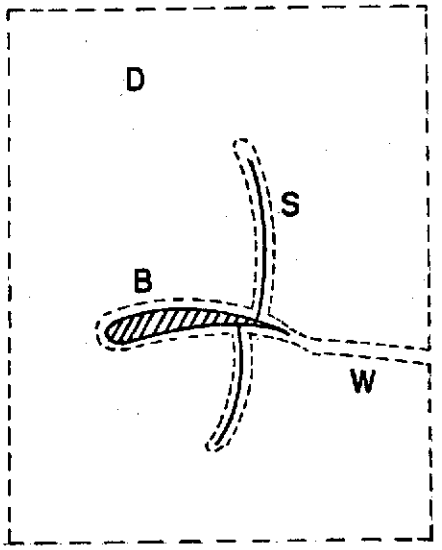

$$\Delta s/c_v = \frac{\gamma^2 - 1}{12\,\gamma^2} (\hat{P}/P - 1)^3 \qquad (22)$$

The pressure jump $(\hat{P}/P) - 1$ can be replaced by the velocity jump through

$$\begin{aligned} \hat{P}/P - 1 &= \{(\hat{P}/P_\infty)/(P/P_\infty) - 1\} \\ &= \{1 + \gamma/2\, M_\infty^2 (-2\,\hat{u}'/U_\infty)\}\{1 + \gamma/2\, M_\infty^2 (-2\,u'/U_\infty)\} - 1 \\ &\doteq -\gamma M_\infty^2 (\hat{u}'/U_\infty - u'/U_\infty) , \end{aligned} \qquad (23)$$

or

$$(\hat{P}/P-1)^3 \doteq -\gamma^3 M_\infty^6 (\hat{u}'/U_\infty - u'/U_\infty)^3 = -\frac{\tau^2 \gamma^3 M_\infty^4}{2\Gamma_1} (\hat{\phi}_x - \phi_x)^3. \qquad (24)$$

After substituting (22) and (24) into (21), we have

$$D = \frac{-\rho_\infty U_\infty^2 M_\infty^2 \tau^{5/3}}{12\,(2\Gamma_1 M_\infty^2)^{1/3}} \int_{\text{shocks}} (\hat{\phi}_x - \phi_x)^3\, d\eta . \qquad (25)$$

Once the shock jump $\hat{\phi}_x - \phi_x$ is accurately calculated by a shock-fitting scheme, the drag can easily be evaluated from (25). A different approach in deriving (25) can be found in Murman and Cole (1974).

4. Applications and further research

Most two-dimensional problems with shock waves can be studied by the present shock-fitting scheme. For flow problems with multiple shocks, special care has to be paid to the region where shock waves merge or intersect each other. For three dimensional problems, the scheme becomes more complicated; we intend to try a simple, finite span wing problem, with shock waves determined by the converged second-order solution. We also intend to compare the result of our scheme with Moretti's three-dimensional shock-fitting result (1973).

At present, we are improving our calculation of flow over a two-dimensional airfoil using the shock-fitting scheme we have developed. For the caustic problem we already studied, numerical computations with a much finer mesh near the triple point will be tested. The goal of the present research is to generalize the present numerical procedure to be useful for most two-dimensional and some simple three-dimensional flow problems.

5. References

Gill, P. M. and Seebass, A. R., 1974, Nonlinear Acoustic Behavior at a Caustic: An Approximate Analytical Solution. Proceedings, AIAA Aero-Acoustics Conference, Seattle, Washington (to appear).

Knechtel, E. D., 1959, Experimental Investigation at Transonic Speeds of Pressure Distributions over Wedge and Circular-Arc Airfoil Sections and Evaluation of Perforated-Wall Interference. NASA TN D-15.

Moretti, G., 1972, Thoughts and Afterthoughts about Shock Computations. Polytechnic Institute of Brooklyn, PIBAL Report No. 72-37.

Moretti, G., 1973, Experiments in Multi-Dimensional Floating Shock-Fitting. Polytechnic Institute of Brooklyn, PIBAL Report No. 73-18.

Murman, E. M. and Cole, J. D., 1971, Calculation of Plane Transonic Flows. AIAA J. Vol. 9, pp. 114-121.

Murman, E. M., 1974, Analysis of Embedded Shock Wave Calculated by Relaxation Methods. AIAA J., Vol. 12, pp. 626-633.

Murman, E. M. and Cole, J. D., 1974, Inviscid Drag at Transonic Speeds. AIAA Paper No. 74-540.

Seebass, A. R., Murman, E. M., and Krupp, J. A., 1971, Finite Difference Calculation of the Behavior of a Discontinuous Signal Near a Caustic. Sonic Boom Research, NASA SP-255, pp. 361-372.

Zierep, V. J., 1958, Der senkrechte Verdichtungsstoss am gekrümmten Profil. ZAMP, Vol. IXb, 1958, pp. 764-776.

Appendix

A

Abstract

This paper discusses the procedures we have developed to treat a canonical problem involving a mixed nonlinear equation with boundary data that imply a discontinuous solution. This equation arises in various physical contexts and is basic to the description of the nonlinear acoustic behavior of a shock wave near a caustic. The numerical scheme developed is of second order, treats discontinuities as such by applying the appropriate jump conditions across them, and eliminates the numerical dissipation and dispersion associated with large gradients. Our results are compared with the results of a first-order scheme and with those of a second-order scheme we have developed. The algorithm used here can easily be generalized to more complicated problems, including transonic flows with imbedded shocks.

Introduction

The computation of mixed, e.g., transonic, flows has been investigated extensively in the past decade. Recent surveys of the numerical procedures used can be found in Nieuwland and Spee (1973), and Yoshihara (1972). The numerical treatment of such flows when shock waves are present has not been developed satisfactorily. Recently, Murman (1974) improved previous relaxation procedures by introducing a "shock point operator" to the difference equations. His scheme notes the local character of the flow, and provides a relaxation scheme that insures that the calculation is fully conservative. However, due to first-order truncation errors, shock waves are smeared out, and consequently shock wave geometry can not be accurately predicted. We present a numerical procedure for solving mixed equations with second-order numerical accuracy by treating discontinuities as such. Moretti (1969 , 1972, 1973) has pursued a similar course in tackling related problems.

Governing Equation and Boundary Conditions

We consider

$$(y + \phi_x)\,\phi_{xx} - \phi_{yy} = 0 \qquad (1)$$

where ϕ may be thought of as a (perturbed) velocity potential, with boundary data prescribed in accordance with the nonlinear generalization of properly posed problems for

$$y\,\phi_{xx} - \phi_{yy} = 0. \tag{2a}$$

Numerical boundary data are determined from the solution to (2a) for an incoming signal with

$$\phi_x \sim -\mu y^{-1/4} F(p)\ , \text{ for } q \to -\infty\ , \tag{2b}$$

where $F(p)$ gives the shape of an incoming signal, μ characterizes its strength, and p, $q = x \pm 2/3\ y^{3/2}$, respectively. Equation (1) arises in various physical contexts; one of these is discussed in some detail in Seebass (1971). A discontinuous signal with strength $\mu = 0.05$ was chosen for the present study with

$$F(p) = H(p) - H(p + \delta), \tag{2c}$$

where $H(p)$ is the Heaviside unit function, and δ was taken to be 20. This problem is sketched in figure 1 for the domain considered here.

The characteristic directions and the corresponding compatibility relations for (1) are

$$dy/dx = \pm\,(y + \phi_x)^{-1/2}\ , \tag{3}$$

$$(y + \phi_x)^{1/2}\, d\phi_x = \pm\, d\phi_y\ . \tag{4}$$

If discontinuities are present in the solution of (1), then they must have the directions

$$dy/dx = \pm\,\{y + \tfrac{1}{2}\,(\phi_x + \hat{\phi}_x)\}^{-1/2} \tag{5}$$

and across them

$$(\hat{\phi}_x - \phi_x)^2\{y + \tfrac{1}{2}\,(\phi_x + \hat{\phi}_x)\} = (\hat{\phi}_y - \phi_y)^2 \tag{6}$$

where, e.g., $\hat{\phi}_x - \phi_x$ is the jump in ϕ_x across the discontinuity.

Solutions to the linear problem (2) may be calculated with any precision desired (Gill and Seebass, 1974). Values of ϕ_x for fixed y are displayed in figure 2. The results provide an initial guess of the solution to (1), as well as the boundary data. The computation is carried out in the region of figure 1. At points on the boundary where $y + \phi_x < 0$, ϕ is prescribed; at appropriate points on the boundary where $y + \phi_x > 0$, ϕ and ϕ_x are prescribed. On certain portions of the boundary, no data are prescribed because the solution is determined uniquely without them.

A first-order numerical "solution" to (1) was obtained by Seebass, Murman, and Krupp (1971) with an implicit, backward difference approximation to x-derivatives chosen for the grid points that lie in the hyperbolic region. The scheme is unconditionally stable and the numerical calculations converge. However, the "solution" does not give a satisfactory representa-

tion of the discontinuities. We have developed a modified second-order scheme that solves (1), the smeared "discontinuities" obtained are considerably thinner than those obtained from the first-order scheme. One drawback of the second-order scheme is that in certain regions dispersive errors dominate and an unpleasant "wiggle" appears on the "downstream" side of the discontinuity. Using these second-order results for initial conditions, we then proceed with a second-order "shock-fitting" scheme that treats the discontinuities as such in order to satisfy the jump conditions to second-order.

Numerical Procedure

Second-Order Scheme

The difference equations for (1) are of the form

$$A_1\ \phi_{i,j+1}^{n+1} + A_2\ \phi_{i,j}^{n+1} + A_3\ \phi_{i,j-1}^{n+1} + A_5 = 0 \tag{7}$$

or $F_j(\phi) = 0$, where the index "i" refers to grid points in the x-direction, "j" to the grid points in the y-direction, and the superscript "n+1" to the number of iterations of the entire region. The coefficients, An, are listed in table 1. Equation (7) is linear in elliptic domains, and nonlinear in hyperbolic domains and can be solved by Newton's method, i.e.,

$$\phi^{n+1} - \phi^{n} = -\{\partial F_j(\phi)/\partial\phi_k\}^{-1}\ F_j(\phi). \tag{8}$$

The difference approximation displayed in table 1 has the truncation error

$$\begin{aligned} &\frac{5}{6}\,\Delta x^2\ \phi_{xx}\phi_{xxx} + \frac{11}{12}\,\Delta x^2(y + \phi_x)\phi_{xxxx} + \frac{1}{12}\,\Delta y^2\phi_{yyyy}, \text{ for } y + \phi_x > 0, \\ &-\frac{1}{6}\,\Delta x^2\ \phi_{xx}\phi_{xxx} - \frac{1}{12}\,\Delta x^2(y + \phi_x)\phi_{xxxx} + \frac{1}{12}\,\Delta y^2\phi_{yyyy}, \text{ for } y + \phi_x < 0. \end{aligned} \tag{9}$$

Special care has to be taken when Newton's method is applied to hyperbolic domains. For hyperbolic equations the numerical error will not decay unless a proper scheme has been used. In the present problem the diagonal term of the tri-diagonal matrix $\partial F_j(\phi)/\partial\phi_k$ for hyperbolic domains is of the form

$$\begin{aligned} \text{Diag}(j) &= \frac{2}{\Delta y^2} + \frac{2y}{\Delta x^2} + \frac{2}{\Delta x^3}\ (2\phi_{i,j}^{n+1} - 3\phi_{i-1,j}^{n+1} + \phi_{i-2,j}^{n+1}) \\ &\doteq \frac{2}{\Delta y^2} + \frac{2}{\Delta x^2}\,(y + \phi_x) + \frac{1}{\Delta x}\,\phi_{xx}\ . \end{aligned} \tag{10a}$$

In hyperbolic compressive regions the matrix loses diagonal dominance when

$$\frac{2}{\Delta x^2}\,(y + \phi_x) + \frac{1}{\Delta x}\,\phi_{xx} < 0\ . \tag{10b}$$

This can lead either to poor convergence or to instability of Newton's method. Thus an amendment is made by adding an artificial term $\kappa\phi_{xxx}$, to (1), such that the difference equation remains diagonally dominant in the iterative procedure. The value of κ is of second order, and is determined by

$$\frac{2}{\Delta x^2}(y + \phi_x) + \frac{1}{\Delta x}\phi_{xx} - \frac{\kappa}{\Delta x^3} > 0 \qquad (11)$$

With this modification, a stable second-order numerical solution is obtained. Computer-drawn plots of $-\phi_x/\mu$ at constant y are shown in figure 3. When these results are compared with the first-order computation shown in figure 4, it can be seen that the second-order scheme provides sharper and thinner "shocks". However, as mentioned, in regions where $|y + \phi_x| > |\phi_{xx}|$, "wiggles" appear.

Shock-Fitting Technique

Moretti (1972) has emphasized the importance of treating discontinuities as such for flows containing shock waves. He calls this procedure "shock fitting". Without shock fitting, a large number of grid points and considerable computing time are required to achieve a given accuracy. The advantage of shock fitting is clearly demonstrated by the present study. With shock fitting, we can determine both the shock position and the shock pressure rise with reasonable accuracy. Moreover, effects of numerical dissipation and dispersion are reduced to a minimum.

We assume the computation procedure has reached station "i", i.e., $x = x_i$, as shown in the sketch of table 2; the upstream conditions are then all known, and the properties of the downstream shock point "b" can be calculated by using the characteristic relations along bd, be, bf, and the jump condition (6). At point "c", where the shock intersects vertical grid line $x = x_i$, the value of ϕ is calculated by direct integration of $d\phi$ along bc. We then construct the difference approximation to x, and y derivatives by using the shock points b and c instead of the regular grid points, e.g., h and k. Again, an implicit scheme is used when the equation is hyperbolic and a central-difference scheme when it is elliptic. During the computation the position of the shock is determined and the quantity $y + \phi_x$ is computed at each grid point so that the proper difference equations can be selected.

As the incident discontinuity approaches the line where $y + \phi_x = 0$ it grows in strength until the flow right behind the incident wave becomes sonic. At that point we have assumed that a reflected wave is formed. The initial strength of the reflected wave can be obtained either by constructing local symmetrical discontinuities that meet at this point (a triple point), or by using backward differences to approximate properties ahead of the shock and using forward differences to approximate properties behind the shock. The second method is easier to use and the present study is limited to it. The strength of the discontinuity increases rapidly and approaches its final value within 5 to 10 iterations. Computer-drawn plots of $-\phi_y/\mu$ at constant y are shown in figure 5. The reflected discontinuity is weak, but this may be due, in part, to the procedure we invoked at the

triple point. However, the reflected wave is not weak and is poorly represented by the second-order results without shock fitting.

Conclusion

The numerical scheme outlined here offers a reliable method of computing solutions to the mixed nonlinear equations with discontinuities. Comparison of the graphical results for different schemes shows the present method provides quantitatively superior results for an equal investment in computational time.

Stability criteria for shock-fitting procedures derive from the same arguments used for the first-order and second-order implicit scheme. The rate of convergence may be studied by examining the maximum error of ϕ for each successive calculation along column x_{im} which requires the maximum number of iterations to compute, i.e.,

$$\text{Maximum error} = \max_{j=1,J} |1 - \phi^{n+1}_{i,j}/\phi^{n}_{i,j}| \text{ along } x_{im} .$$

Table 3 compares the computation time and the maximum error for the first-order, the second-order, and the shock-fitting schemes. It can be seen that for 60 iterations both the first-order and the second-order schemes have approximately the same rate of convergence. The initial guess was the linear solution for both calculations. We can not use the linear solution as initial data with shock-fitting because the linear solution is too poor an initial guess. Our computation used the results from the second-order scheme as initial data. It took only twenty computations to reduce the maximum error to 1%. The fast rate of convergence probably derives from the accuracy of the second-order solution away from the discontinuities, but it also indicates the efficiency of our procedure. The most undesirable feature of the shock-fitting scheme is that the program becomes complicated with bookkeeping. However, for two-dimensional problems, even those with multiple discontinuities, the present scheme seems easy to apply. For three-dimensional problems the difficulties are more substantial.

Acknowledgements

The authors would like to thank Dr. E. M. Murman for constructive criticism of this research, which was supported by the NASA through grant NGR 030-010-057.

References

Gill, P.M. and Seebass, R., 1974, Nonlinear Acoustic Behavior at a Caustic: An Approximate Analytical Solution. Proceedings, AIAA Aero-Acoustics Conference, Seattle, Washington (to appear).

Moretti, G., 1969, A Critical Analysis of Numerical Techniques: The Piston-Driven Inviscid Flow. Polytechnic Institute of Brooklyn, PIBAL Report 69-25.

Moretti, G., 1972, Thoughts and Afterthoughts about Shock Computations, Polytechnical Institute of Brooklyn, PIBAL Report No. 72-37.

Moretti, G., 1973, Experiments in Multi-Dimensional Floating Shock-Fitting. Polytechnic Institute of Brooklyn, PIBAL Report No. 73-18.

Murman, E.M., 1974, Analysis of Embedded Shock Waves Calculated by Relaxation Methods, AIAA J. Vol. 12, pp. 626-633.

Nieuwland, G.Y. and Spee, B.M., 1973, Transonic Airfoils: Recent Developments in Theory, Experiment, and Design. Annual Review of Fluid Mechanics, pp. 119-150.

Seebass, A.R., 1971, Nonlinear Acoustic Behavior at a Caustic, Sonic Boom Research, NASA SP-255, pp. 87-122.

Seebass, A.R., Murman, E.M., and Krupp, J.A., 1971, Finite Difference Calculation of the Behavior of a Discontinuous Signal Near a Caustic, Sonic Boom Research, NASA SP-255, pp. 361-372.

Yoshihara, Y., 1972, A Survey of Computational Methods for 2-D and 3-D Transonic Flows with Shocks. Convair Aerospace Division, General Dynamics, Report GDCA-ERR-1726.

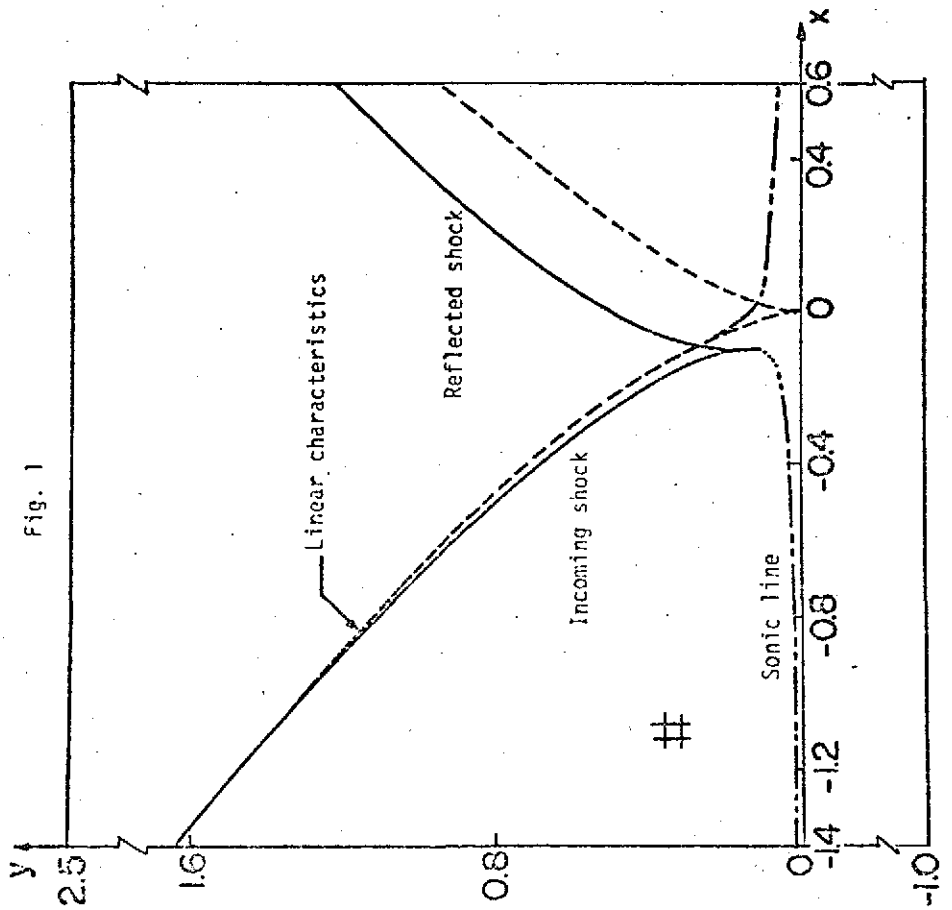

Fig. 1

Sketch of computation region, shock waves and sonic line. The computation region is divided into 51 grid points in the x-direction and 71 grid points in the y-direction. Thus $\Delta x = 0.04$ and $\Delta y = 0.05$.

Fig. 2

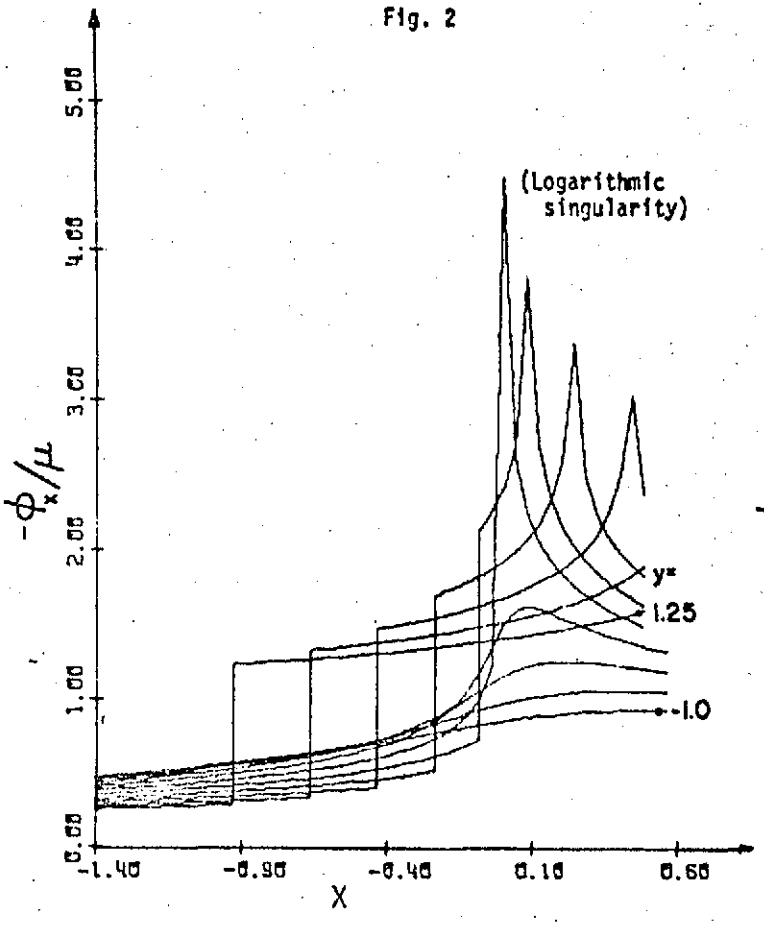

Computer drawn plots of $-\phi_x/\mu$ at constant y for the linear solution. Increments in y are 0.25.

Fig. 3

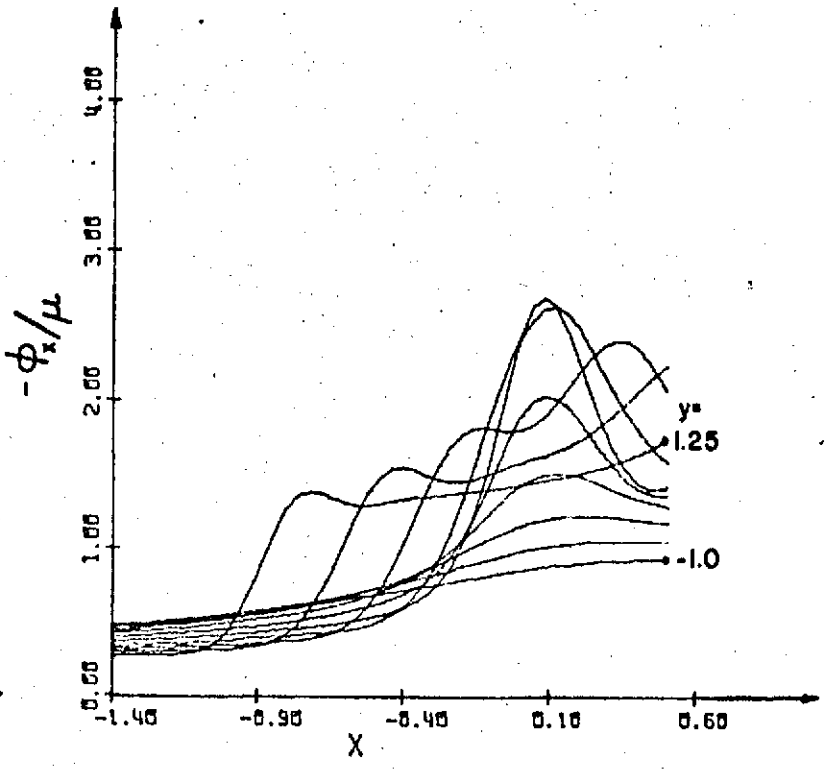

Computer drawn plots of $-\phi_x/\mu$ at constant y for the second-order calculation. Increments in y are 0.25.

Fig. 4

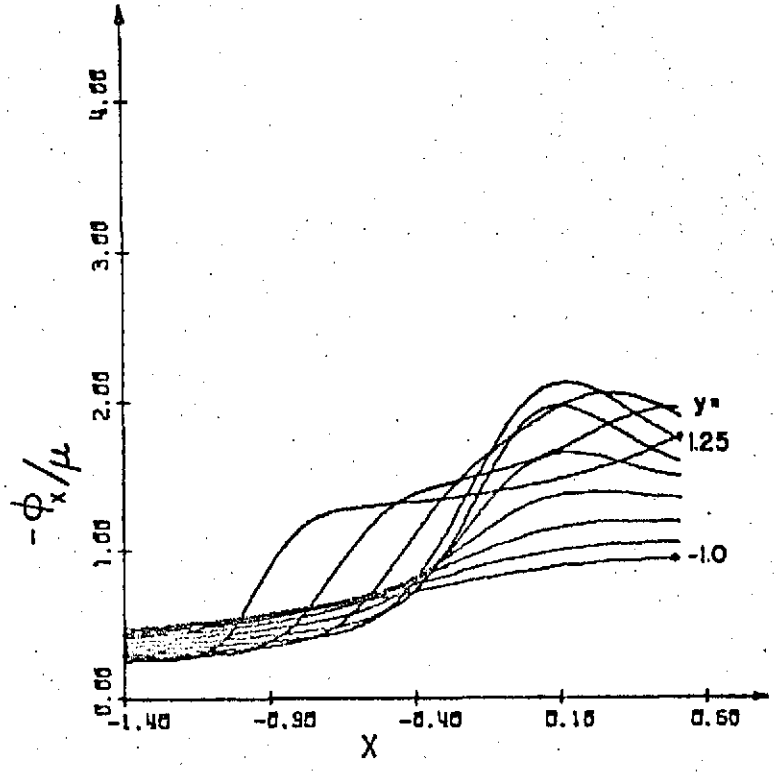

Computer drawn plots of - ϕ_X/μ at constant y for a first-order calculation. Increments in y are 0.25.

Fig. 5

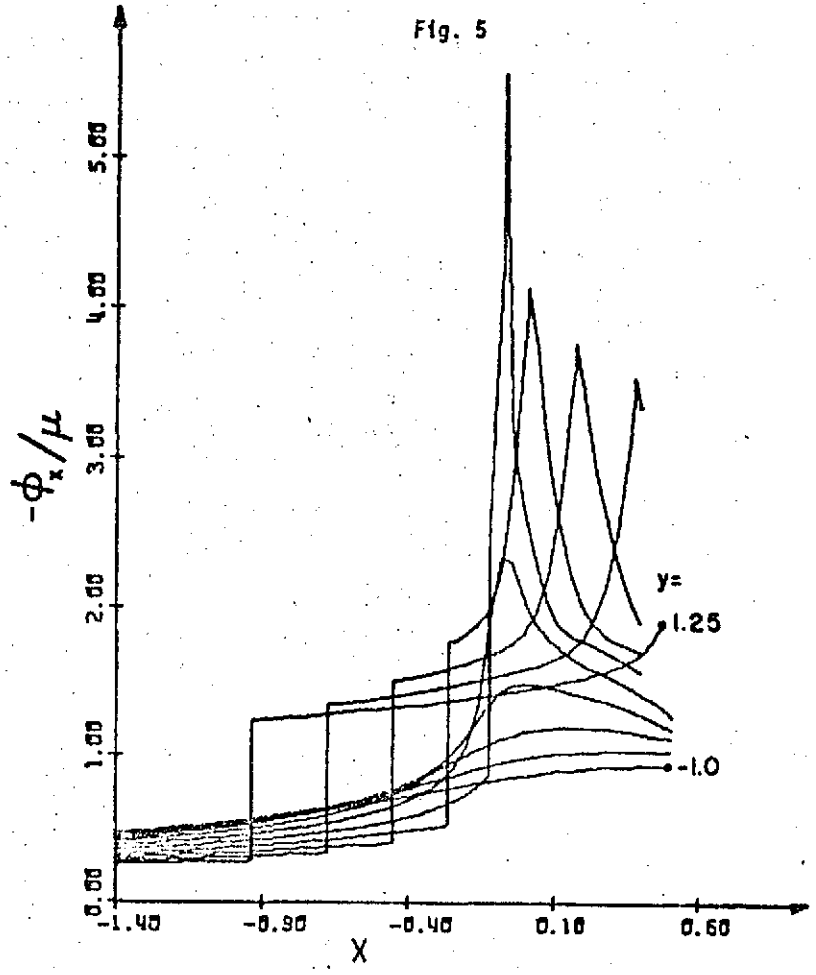

Computer drawn plots of - ϕ_X/μ at constant y with shock fitting. Increments in y are 0.25.

Table 1. Formulation of Difference Equations

$$A_1 \phi^{n+1}_{i,j+1} + A_2 \phi^{n+1}_{i,j} + A_3 \phi^{n+1}_{i,j-1} + A_4 \phi_s + A_5 = 0$$

Case 1. Shock-free region:

$$(y+\phi_x)\phi_{xx} = \frac{1}{\Delta x^2}\begin{cases} 2[y + \frac{1}{\Delta x}(\phi^{n+1}_{i,j} - 3\phi^{n+1}_{i-1,j} + \phi^{n+1}_{i-2,j})]\phi^{n+1}_{i,j} + (-5\phi^{n+1}_{i-1,j}+4\phi^{n+1}_{i-2,j}-\phi^{n+1}_{i-3,j}) \\ \quad \cdot [y - \frac{1}{2\Delta x}(\phi^{n+1}_{i-1,j} - 2\phi^{n+1}_{i-2,j} - \phi^{n+1}_{i-3,j})], & y+\phi_x > 0 \\ 0, & y+\phi_x = 0 \\ [-2y - \frac{1}{\Delta x}(\phi^{n}_{i+1,j} - \phi^{n+1}_{i-1,j})]\phi^{n+1}_{i,j} + (\phi^{n}_{i+1,j} + \phi^{n+1}_{i-1,j})\left[y + \frac{1}{2\Delta x}(\phi^{n}_{i+1,j} - \phi^{n+1}_{i-1,j})\right], & y+\phi_x < 0 \end{cases}$$

$$\phi_{yy} = \frac{1}{\Delta y^2}(\phi^{n+1}_{i,j+1} - 2\phi^{n+1}_{i,j} + \phi^{n+1}_{i,j-1}) \text{ , for } y + \phi_x \gtrless 0.$$

Case 2. Shock region:

$$(y+\phi_x)\phi_{xx} = \begin{cases} \frac{1}{a^2}[y + \frac{1}{a}(\phi^{n+1}_{i,j} - 2\phi^{n+1}_{s} - a\hat{\phi}^{n+1}_{x_s})]\phi^{n+1}_{i,j} - \frac{1}{a^2}(y - \frac{1}{a}\phi^{n+1}_{s})(\phi^{n+1}_{s} - a\hat{\phi}^{n+1}_{x_s}), & 0 < x_i - x_s \leq \Delta x \\ [E_1(E_5\phi^{n+1}_{i-1,j} + E_6\phi^{n+1}_{i-2,j} + E_5(y+E_2\phi^{n+1}_{i-1,j}+E_3\phi^{n+1}_{s})+E_1E_4\phi^{n+1}_{i,j}]\phi^{n+1}_{i,j} \\ \quad + (y+E_2\phi^{n+1}_{i-1,j}+E_3\phi^{n+1}_{s})(E_5\phi^{n+1}_{i-1,j}+E_6\phi^{n+1}_{s}), & \Delta x < x_i - x_s \leq 2\Delta x \\ [D_1(D_6\phi^{n+1}_{i-1,j}+D_7\phi^{n+1}_{i-2,j}+D_8\phi^{n+1}_{s})+D_5(y+D_2\phi^{n+1}_{i-1,j}+D_3\phi^{n+1}_{i-2,j}+D_4\phi^{n+1}_{s})+D_1D_5\phi^{n+1}_{i,j}]\phi^{n+1}_{i,j} \\ \quad + (y+D_2\phi^{n+1}_{i-1,j}+D_3\phi^{n+1}_{i-2,j}+D_4\phi^{n+1}_{s})(D_6\phi^{n+1}_{i-1,j}+D_7\phi^{n+1}_{i-2,j}+D_8\phi^{n+1}_{s}). & 2\Delta x < x_i - x_s \leq 3\Delta x \end{cases}$$

$$\phi_{yy} = \begin{cases} \frac{1}{\Delta y^2}(\phi^{n+1}_{i,j+1} - 2\phi^{n+1}_{i,j} + \phi^{n+1}_{i,j-1}), & \text{Regular point} \\ \frac{2}{d(d+\Delta y)}\phi^{n+1}_{s} - \frac{2}{d\Delta y}\phi^{n+1}_{i,j} + \frac{2}{\Delta y(d+\Delta y)}\phi^{n+1}_{i,j-1}, & y_j \leq y_s < y_{j+1},\ d = y_s - y_j \\ \frac{2}{\Delta y(e+\Delta y)}\phi^{n+1}_{i,j+1} - \frac{2}{e\Delta y}\phi^{n+1}_{i,j} + \frac{2}{e(e+\Delta y)}\phi^{n+1}_{s}, & y_{j-1} < y_s < y_j,\ e = y_j - y_s \end{cases}$$

Here $a = x_i - x_s$, the D_n, E_n are coefficients determined by appropriate Taylor series expansions. The A_n are obtained from the appropriate choice of the above representations.

Table 2. Illustration of Shock Fitting

Position of shock point b:

$$\frac{x_b - x_a}{y_b - y_a} = -\left\{ y + \frac{1}{2}(\phi_x + \hat{\phi}_x) \right\}_{ab}^{1/2}$$

Properties ahead of the shock:

$$\phi_{x_b} = \frac{1}{(y+\phi_x)_{be}^{1/2} + (y+\phi_x)_{bd}^{1/2}} \left\{ (y+\phi_x)_{be}^{1/2} \phi_{x_e} + (y+\phi_x)_{bd}^{1/2} \phi_{x_d} + \phi_{y_d} - \phi_{y_e} \right\}$$

$$\phi_{y_b} = \phi_{y_d} - (y+\phi_x)_{bd}^{1/2} (\phi_{x_b} - \phi_{x_d})$$

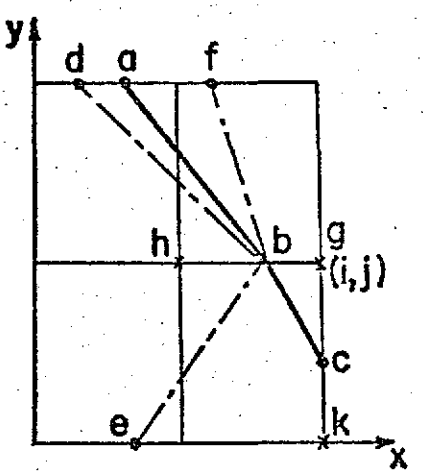

Properties behind the shock:

$$(y+\phi_x)_{bf}^{1/2} (\hat{\phi}_{x_b} - \phi_{x_f}) = \phi_{y_f} - \hat{\phi}_{y_b}$$

$$(\hat{\phi}_{x_b} - \phi_{x_b})^2 \left\{ y + \frac{1}{2}(\phi_{x_b} + \hat{\phi}_{x_b}) \right\} = (\hat{\phi}_{y_b} - \phi_{y_b})^2$$

$$\phi_b = \phi_h + \frac{1}{2}(x_b - x_h)(\phi_{x_h} + \phi_{x_b})$$

Shock point c:

$$\phi_c = \phi_b + \int_b^c d\phi \doteq \phi_b + \hat{\phi}_{x_b}(x_c - x_b) + \hat{\phi}_{y_b}(y_c - y_b)$$

Here $( )_{ab}$ means $\frac{1}{2}[( )_a + ( )_b]$.

Table 3. Computation Time and Rate of Convergence

i x j	Scheme	Number of Computations*	Time/Comp.**	Maximum Error
51 x 71	First order	60	4.11 (sec.)	0.039593+
	Second order	60	4.51	0.060134+
	Present	20	9.16	0.010475

*A computation is one complete calculation of the "solution".

**Compiling time excluded.

+Maximum error still fluctuates after 60 computations.